JCTC Journal of Chemical Theory and Computation

ARTICLE

pubs.acs.org/JCTC

Locating Instantons in Many Degrees of Freedom

Judith B. Rommel,[†] T. P. M. Goumans,[‡] and Johannes Kästner*[,†]

[†]Computational Biochemistry Group, Institute of Theoretical Chemistry, University of Stuttgart, Stuttgart, Germany

[‡]Gorlaeus Laboratories, LIC, Leiden University, Leiden, The Netherlands

ABSTRACT: We implemented and compared four algorithms to locate instantons, i.e., the most likely tunneling paths at a given temperature. These allow to calculate reaction rates, including atom tunneling, down to very low temperature. An instanton is a first-order saddle point of the Euclidean action in the space of closed Feynman paths. We compared the Newton−Raphson method to the partitioned rational function optimization (P-RFO) algorithm, the dimer method, and a newly proposed mode-following algorithm, where the unstable mode is directly estimated from the instanton path. We tested the algorithms on three chemical systems, each including a hydrogen transfer, at different temperatures. Overall, the Newton−Raphson turned out to be the most promising method, with our newly proposed mode following, being the fall-back option.

I. INTRODUCTION

Quantum tunneling of atoms plays an important role in many chemical reactions, predominantly those involving hydrogen atoms. Especially at low temperature, tunneling increases reaction rates compared to a nonquantum mechanical over-the-barrier model.

The tunneling probability depends on the mass of the particles that undergo tunneling motion and on the shape and height of the effective barrier being crossed.[1,2] The mass dependence of the tunneling rate gives rise to large kinetic isotope effects (KIE). Atom tunneling is observed in reactions in space,[3−5] in biological applications,[6−9] and in other areas of chemistry. In principle, any chemical reaction will be dominated by tunneling at low enough temperature.

Many enzymes support tunneling of hydrogen atoms even at room temperature. Experimentally, this is observed by an unusually large KIE,[6,9−13] the ratio between the reaction rates involving deuterium and protium. In computer simulations, the importance of tunneling can directly be shown by switching the effect on or off.[7,8,14−17] A high KIE only shows that tunneling accelerates the rate-limiting step of a reaction. There is an active debate as to whether the tunneling process of atoms is crucial for the catalytic effect of some enzymes and whether it is actively promoted by the proteins. Calculations are a promising tool to provide insight into these issues.

In classical transition-state theory (TST),[18,19] reviewed in refs 20 and 21, quantum effects can be included via the vibrations (and, thus, the zero-point energy). However, tunneling is neglected. A general transition state in a system with N degrees of freedom is a closed $N-1$-dimensional hypersurface encapsulating the reactant state. Commonly, however, one refers to a (classical) transition state as a first-order saddle point on the potential energy surface. The latter meaning will be used here.

In the following, we give a short overview of methods to calculate tunneling rates. Since many methods have appeared over the years, this list is necessarily incomplete.

Tunneling near the top of the barrier is accounted for by corrections to the classical reaction rate proposed by Wigner[22] and used by Bell.[23] The classical rate is multiplied by a correcting factor $\kappa(T)$, which results in exact rates for parabolic barriers. The method is applicable above a crossover temperature T_c:[24]

$$T_c = \frac{\hbar\Omega}{2\pi k_B} \tag{1}$$

where Ω denotes the magnitude of the imaginary frequency of the unstable mode at the saddle point. To extend the range of applicability to below T_c, a third-order expansion in $\hbar$ of $\kappa(T)$ was used.[25]

The semiclassical approximation assumes one main tunneling path rather than taking the whole potential energy surface into account. Methods based on the transition-state theory and the semiclassical approximation can be categorized by their choice of the tunneling path. The zero-curvature tunneling approximation (ZCT)[26] approximates the tunneling path by the intrinsic reaction path (minimum-energy path (MEP) in mass-weighted coordinates). Even at rather high temperature, close to T_c, the most likely tunneling path will, however, deviate from the MEP. The effect is known as corner cutting.[27] Small-curvature tunneling (SCT)[28] assumes a tunneling path in the vicinity of the MEP. SCT can be expected to be a good approximation close to T_c. The other extreme for a choice of a tunneling path is the straight line path in a method known as large curvature tunneling correction (LCT).[29,30] While minimizing the tunneling distance, LCT ignores the potential energy in the choice of the path. At low temperature, LCT can be expected to be a better approximation than SCT. It has been proposed[31,32] to use a linear combination of the SCT and LCT paths by minimizing the tunneling action.

The optimal tunneling path within the purely statistical semiclassical approximation is found by the instanton method,[33−37] analogous to the imaginary F method.[33] It is based on statistical Feynman path integrals.[38] Some of the aforementioned approximations can be regarded as an approximation to the instanton method. The instanton itself is the tunneling path with the

Received: November 15, 2010
Published: February 18, 2011

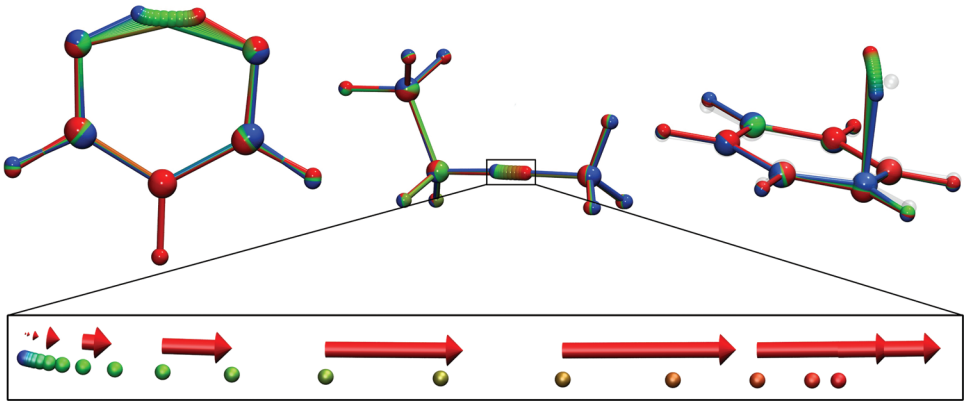

Figure 1. top: Instanton geometries of the three test cases: malonaldehyde, ammonium and methylamine as well as H + benzene. Each calculated at T = 200 K with P = 20 images. Bottom: the transition mode $\mathbf{u}_{\mathrm{inst}}$ indicated as arrows on the hydrogen atom transferred between ammonium and methylamine. For clarity, only the arrows corresponding to every second image are shown. The components of $\mathbf{u}_{\mathrm{inst}}$ on the other atoms are negligibly small on the scale shown.

highest statistical weight at a given temperature. Due to a mathematical equivalence, it can also be interpreted as a periodic orbit in the upside-down potential energy surface of the system. In the formulation of a harmonic quantum transition-state theory, many parallels between the classical TST and the instanton method were demonstrated.[39] It is, along with some extensions,[40,41] increasingly used to calculate reaction rates in chemical systems.[4,5,42−50]

Beyond TST, quantum dynamics allows to calculate tunneling rates by solving the time-dependent Schrödinger equation. The time-dependent Hartree approach[51−54] and other methods[55,56] were proposed. The costs of these methods grow exponentially with the number of degrees of freedom. Statistical Feynman paths can circumvent that and have also been used in simulations to estimate dynamical properties either by evaluating a centroid potential of mean force[57−60] or by so-called ring polymer dynamics.[61] Feynman path integral approaches using TST, but not the semiclassical approximation, are also in use. The centroid density method, a quantum transition-state theory (QTST), is one of these.[24,62,63] Another QTST approach is the reversible action-space work QTST (RAW-QTST),[39,45] which in the harmonic limit reduces to instanton theory.

This paper is organized as follows. In Section II we describe the details of instanton theory. In Section III we propose possible techniques to locate instantons. In Section IV we compare the efficiency of these algorithms for a series of test systems at different temperature. In Section V we discuss the efficiency of the algorithms, possible issues which may impede instanton optimizations, and ways to avoid them. Finally, we conclude and give an outlook at more realistic calculations as well as further problems which remain to be solved.

II. INSTANTON THEORY

The quantum statistical partition function Q is expressed via a Feynman path integral:[38]

$$Q = \int \mathrm{d}x \, \langle x|\exp^{-\beta H}|x\rangle = \int \mathrm{d}x \int_{\bar{x}(0)=x}^{\bar{x}(\beta\hbar)=x} \mathcal{D}\bar{\mathrm{x}} \exp\left(-\frac{1}{\hbar}S_{\mathrm{E}}[\bar{\mathrm{x}}]\right) \qquad (2)$$

with $\beta = 1/(k_{\mathrm{B}}T)$, H the Hamiltonian of the system, and k_{B} being Boltzmann's constant. $\mathcal{D}\bar{x}$ has the "heuristic" meaning of integration over all paths $\bar{\mathrm{x}}$ satisfying the boundary conditions $\bar{x}(0) = \bar{x}(\beta\hbar) = x$. $\mathcal{D}\bar{x}$ can be formed into a conditional Wiener measure to give a well-defined formulation of the integral.[64] Here and in the following, points in configuration space (N dimensional for a molecule with N degrees of freedom) are denoted by italic symbols (x), while paths are denoted by upright (roman) symbols (x). The Euclidean action functional S_{E} is given by

$$S_{\mathrm{E}}[\bar{x}] = \int_0^{\beta\hbar} \left(\frac{m}{2}\frac{\mathrm{d}\bar{x}(\tau)^2}{\mathrm{d}\tau} + V(\bar{x}(\tau))\right)\mathrm{d}\tau \qquad (3)$$

with $V(x)$ being the potential energy.

To approximate the integral over all paths in eq 2, S_{E} is expanded to second order around its stationary paths. The stationary condition is

$$\left[\frac{\delta S_{\mathrm{E}}}{\delta \bar{x}}\right]_{x_0} = -m\frac{d^2x_0(\tau)}{\mathrm{d}\tau^2} + \nabla V(x_0(\tau)) = 0 \qquad (4)$$

One path which fulfills eq 4 is x collapsed to the geometry of the reactant minimum ($\bar{x}(\tau) = x_{\mathrm{RS}}$). From this, the quantum partition function of the reactant can be obtained. To use transition-state theory, the partition function of a quantum transition state (QTS), a dynamical bottleneck between the reactant and the product, is required. In contrast to the path corresponding to the reactant minimum, the instanton path $\mathrm{x}_{\mathrm{inst}}$ is delocalized. Its Hessian exhibits exactly one negative eigenvalue, the eigenvector $\mathbf{u}_{\mathrm{inst}}$ corresponding to a movement of the whole path toward the reactant or the product. An example of $\mathbf{u}_{\mathrm{inst}}$ is depicted in Figure 1. The Hessian of the instanton additionally exhibits one eigenvalue which is 0. This corresponds to the arbitrary starting position of the path, i.e., to a reparametrization $\tau \rightarrow \tau + c$ of the path. For molecules, the Hessian exhibits another six 0 eigenvalues (5 for linear molecules), corresponding to the translation and rotation of the whole molecule.

To calculate the Euclidean action and, through that, the rate the Feynman path $x(\tau)$ is discretized into P' images. By introducing mass-weighted coordinates $y_i = x_i(m_i)^{1/2}$ the equation can be somewhat simplified

$$S_E = \beta\hbar \sum_{k=1}^{P'} \left(\frac{P'}{2(\beta\hbar)^2} |y_{k+1} - y_k|^2 + \frac{V(y_k)}{P'} \right) \quad (5)$$

To fulfill eq 4, a stationary point has to be searched for. Since we are interested in a rate, we specifically search for a first-order saddle point. This saddle point is the instanton.

It turns out that the instanton is delocalized along one line in the configuration space of the molecule. The Feynman path is closed by proceeding along this line forward and backward. Choosing an even number of images and starting the index $k = 1$ at an image next to one turning point, the images k and $P' - k + 1$ have identical coordinates. All images are traversed twice, the turning points lie outside of the discretized path. Thus, it is sufficient to sum over half of the images ($P = P'/2$):[65]

$$S_E = \frac{2P}{\beta\hbar} \sum_{k=1}^{P-1} |y_{k+1} - y_k|^2 + \frac{\beta\hbar}{P} \sum_{k=1}^{P} V(y_k) \quad (6)$$

Equation 6 can be used to derive the gradient and the Hessian of S_E with respect to the coordinates of the atoms of each image.

The problem of finding an instanton has been formulated here as a saddle-point search of a discretized path. This allows to treat a high number of degrees of freedom. Instantons can, however, also be interpreted as unstable periodic orbits on the upside-down potential energy surface ($-V$). Techniques to find periodic orbits[66,67] have previously been used to find instantons.[68,69] In practice, these techniques are, however, only applicable to systems with a few degrees of freedom.[69]

The integral over all paths in eq 2 is approximated by expanding $V(x)$ at each point, and, thus, $S_E[\mathrm{x}]$ quadratically around the stationary path x_{inst}. Then the integral in eq 2 turns into a Gaussian integral which can be solved analytically. This results in an expression of the rate:[34,36,70]

$$k_{inst} = \frac{1}{Q_{RS}} \sqrt{\frac{S_0}{2\pi\hbar}} \frac{P'}{\beta\hbar} \frac{1}{\sqrt{|\Pi_i' \lambda_i|}} \exp(-S_E[\mathrm{x}_{inst}]/\hbar) \quad (7)$$

with Q_{RS} denoting the quantum mechanical partition function of the reactant state, λ_i are the eigenvalues of the Hessian of S_E, and the prime on the product indicates that the zero eigenvalue(s) are omitted. S_0 is twice the part of the Euclidean action depending on the length of the path:

$$S_0 = \frac{4P}{\beta\hbar} \sum_{k=1}^{P-1} |y_{k+1} - y_k|^2 \quad (8)$$

The amount of delocalization of the instanton depends on the temperature. At low temperature (high β), the effective force constant between the images, $P/(\beta\hbar)$, becomes smaller allowing the images to spread further to accommodate a lower potential energy. With increasing temperature, the path becomes more and more localized, finally collapsing to a point (the classical transition state y_{cl}) at the same T_c as given in eq 1. Instanton theory is applicable below T_c.

III. TECHNIQUES TO FIND INSTANTONS

The task is to find a first-order saddle point of S_E in the $P \times N$-dimensional space (for a molecule with N degrees of freedom) of the coordinates of all atoms of all images of the Feynman path.[45] Generally, we use sequential cooling,[4,5,49,50,65] i.e., we start at a temperature below T_c and calculate an instanton and the tunneling rate. Then we successively lower the temperature, starting the search from a converged instanton. Alternative approaches and other starting paths may be used as well.

Consistently with the notation of continuous paths introduced above, N-dimensional quantities like the position of one image y_k or the classical transition mode u_{cl} are denoted by italic symbols. $P \times N$-dimensional quantities like the complete Feynman path y or the transition mode of the instanton u_{inst} are denoted by upright (roman) symbols.

The infrastructure to calculate the Euclidean action and all the methods to optimize instantons described here were implemented in DL-FIND.[71,72] Through the interface to ChemShell,[73,74] they can be used with many quantum chemistry programs as well as classical force fields or quantum mechanics/molecular mechanics (QM/MM) energy expressions.

A. Starting Path. In order to facilitate the search for an instanton, an initial starting path as close as possible to the final instanton is estimated. For $T \geq T_c$ the instanton is collapsed to y_{cl}, the first-order saddle point on the potential energy surface (classical transition state). As the temperature decreases, the images spread out approximately along the classical unstable mode u_{cl}. In the quadratic region of $V(y)$, the images spread like

$$y(\tau) = y_{cl} + \Delta r\, u_{cl} \cos(2\pi\tau/\beta\hbar), \qquad 0 \leq \tau \leq \beta\hbar \quad (9)$$

So, we use the discretized version for P images:

$$y_i = y_{cl} + \Delta r\, u_{cl} \cos\left(\frac{i - 1/2}{P}\pi\right), \qquad 0 < i \leq P \quad (10)$$

The initial spread Δr is chosen manually. It cannot be estimated from y_{cl} or its Hessian. We used $\Delta r = 0.4$ atomic units.

B. Mode-Following Methods. Minimum-mode following is an approach to search for first-order saddle points. The action is minimized in all directions but one, $\mathbf{u}_{inst}$ (Figure 1). Along $\mathbf{u}_{inst}$ the action is maximized. If $\mathbf{u}_{inst}$ is the eigenvector of the Hessian associated with the lowest eigenvalue, such an algorithm converges to a first-order saddle point.

The dimer method[75−77] is a minimum-mode-following algorithm with the transition mode recalculated in what is called dimer rotation in each iteration. Converged rotation provides the correct $\mathbf{u}_{inst}$ without ever requiring the calculation of the Hessian. We implemented an improved version of the dimer rotations.[78] The limited memory version[79,80] of the Broyden−Fletcher−Goldfarb−Shanno (BFGS)[81−84] optimizer was used for translations and rotations. Dimer rotations were optimized until $\mathbf{u}_{inst}$ changed by less than 5° in one rotation. This required dimer rotations only at the start of an optimization run. A tighter convergence criterion for the rotations was tried but lead to an increase in the number of energy evaluations (i.e., a possible saving through fewer translations was lost by more rotation steps). An alternative to the dimer method, which also does not require the Hessian, is the Lanczos method,[85,86] which has been used to locate instantons.[4,5,49,50,65]

For the instanton search problem it turned out that an approximation of $\mathbf{u}_{inst}$ can easily be obtained

$$\mathbf{u}_{inst,i} \approx \mathbf{u}^{TM}_{inst,i} = \frac{1}{2}(y_{i+1} - y_{i-1}) \quad (11)$$

i.e., the transition mode is assumed to be the tangent of the instanton path. Actually, it is the tangent of only half the path and

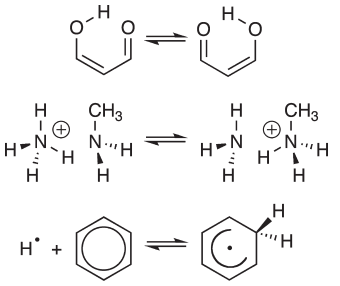

Figure 2. The test cases for which the algorithms to locate instantons were tested: malonaldehyde, ammonium and methylamine, and the addition of hydrogen to benzene.

the reversed tangent of the other half. However, as given in eq 6, we only use the first half of the instanton path as active variables in the optimization. The mode $\mathbf{u}_{\mathrm{inst}}$ is recalculated after each optimization step. Calculating it only at the start and keeping it constant resulted in divergence in some cases. Using a $\mathbf{u}_{\mathrm{inst}}$ calculated by eq 11 is called "tangent mode" (TM) in the following.

C. Hessian-Based Methods. The evaluation of the prefactor of the rate in eq 7 requires to calculate the Hessian of the potential energy surface at each image of the instanton—a computationally demanding task. In sequential cooling it can be used as a good first approximation to the Hessian of the instanton at a lower temperature, which speeds up convergence considerably.

We tested a truncated Newton−Raphson (NR) algorithm and the partitioned-rational function optimizer (P-RFO).[87−90] NR generally converges quadratically to stationary points. However, it has the disadvantage that it converges to any stationary point, not necessarily to first-order saddle points. This is expected unproblematic since our starting structures are often already quite close to the sought-after saddle point. After convergence is achieved, the Hessian at the new instanton geometry has to be calculated. Its eigenvalue spectrum confirms whether a first-order saddle point was obtained.

The P-RFO method converges to first-order saddle points by construction. It is generally the method of choice to search for classical transition states due to its fast and reliable convergence properties.

Hessians are obtained for the individual images from previous rate calculations. With a changed temperature, they are used for the subsequent optimization. With changes in coordinates, we update the Hessians of the individual images according to the Bofill scheme.[91] For small steps and a noisy gradient, the update of the Hessian may actually deteriorate it rather than improve it. So we keep the Hessian unmodified if the coordinates of the images change by less than a predefined threshold. Using the initial Hessian without updates results in less stable optimizations.

When the first instanton below T_c is calculated, a previous Hessian calculation along the full instanton path is unavailable. However, we normally evaluate the Hessian of the potential energy surface at the classical TS. We update this Hessian to the initial image positions, again using the Bofill scheme.

IV. EXAMPLES

The performance of the four optimization algorithms was tested on three chemical systems (Figure 2) at various temperature intervals. All systems were described with semiempirical methods. These pose similar challenges to the optimization algorithms (like numeric discontinuities in the potential energy surface due to incomplete SCF convergence) while being orders of magnitude faster than density functional theory or post-Hartree−Fock methods.

The internal hydrogen transfer in malonaldehyde was simulated with the PM3 Hamiltonian.[92] Since the reactant and product states are chemically indistinguishable, this system has a symmetric barrier. Its tunneling behavior has recently been investigated with a variety of methods.[93] The hydrogen transfer between ammonium and methylamine, also described with PM3, is slightly asymmetric. A very asymmetric barrier is found in the addition of hydrogen to benzene. The latter is a relevant model for the formation of H_2 in space.[4,5] We described it with AM1.[94] In order to get a more realistic reactant-state geometry (van der Waals complex), an empirical dispersion correction originally designed for higher-order methods[95] was added (prefactor $S_6 = 1$). Energies and gradients were calculated with MNDO99[96] interfaced to ChemShell[73,74] through DL-FIND. It should be emphasized that the aim of this study is to compare the efficiency of algorithms rather than the reproduction of experimental values. The instantons of the three test cases are depicted in Figure 1. Visualization was done using VMD 1.8.7.[97]

Classical transition states for the three test systems were calculated with the superlinear converging version[78] of the dimer method[75] as implemented in DL-FIND.[71] Mass-scaled coordinates (mass of hydrogen being 1) were used. Convergence was considered to be achieved for the maximum component of the gradient g_{max} being below a tolerance value (convergence criterion) of $g_{\mathrm{tol}} = 10^{-5}$, the root-mean-square (rms) of the gradient being below 6.66×10^{-6}, the maximum component of the predicted step being below 4×10^{-5}, the rms of the predicted step being below 2.66×10^{-5}, and the last change in the energy of the dimer midpoint being below 2.22×10^{-8}, all values in atomic units. The dimer direction, which in mass-scaled coordinates converges to u_{cl}, was converged in each dimer iteration until it changed by less than 1°.

Hessians were calculated by finite differences of the gradients with two steps of 2×10^{-3} (mass-scaled atomic units) in each dimension. The crossover temperature T_c was obtained according to eq 1 as 442.3, 493.9, and 387.2 K for malonaldehyde, ammonium and methylamine, and H + benzene, respectively.

Instanton searches were performed in mass-weighted coordinates with masses consistent with atomic units (electron mass, m_e). That is, the mass of a hydrogen atom (^{1}H) is 1837.15 m_e. This ensures that the masses in eqs 5 and 6 really drop out. On the other hand, this scales all distances up by a factor of 42.695 [= (atomic mass unit/m_e)$^{1/2}$] compared to mass-scaled coordinates as defined above. Thus, g_{tol} has to be smaller by the same factor to achieve equivalent convergence. The convergence criterion for the instanton searches was $g_{\mathrm{tol}} = 10^{-7}$ for the maximum component of the gradient of $S_E/(\beta\hbar)$ in mass-weighted coordinates (g_{max}). Suitable choices for g_{tol} will be discussed in Section V.

In each case, the first instanton was found for $T = 300$ K by starting from the classical transition state and distributing the $P = 20$ images along u_{cl} using $\Delta r = 0.4$ au as described in Section III.A The numbers of steps needed to reach convergence are given in Table 1. In case of malonaldehyde, the instanton search using NR converged back to a state where all images are collapsed to the classical TS. This is obviously a stationary point, but it is not an instanton, i.e., it does not exhibit the correct number of eigenvalues

Table 1. Number of Steps Needed to Reach Convergence for Finding an Instanton at T = 300 K Starting from the Classical TS[a]

system	TM	dimer	P-RFO	NR
malonal.	114 (2280)	112 (6720)	337 (6726)	64 (1280)
ammon.	103 (2060)	107 (6420)	338 (6760)	46 (920)
H + benzene	151 (3020)	355 (19 360)	137 (2740)	11 (220)

[a] number of energy and gradient evaluations in parentheses, $g_{tol} = 10^{-7}$, and $P = 20$.

Table 2. Number of Steps Needed to Reach Convergence in the Different Methods at Different Temperatures[a]

T (K)	P	TM	dimer	P-RFO	NR
Malonaldehyde					
275	20	81 (1620)	83 (4980)	—[d]	4 (80)
250	20	75 (1500)	79 (4740)	—[d]	6 (120)
225	20	72 (1440)	73 (4380)	—[d]	6 (120)
200	20	70 (1400)	68 (4160)	—[d]	17 (340)
100	20	75 (1500)	—[c]	293 (5860)	45 (900)
200	77	275 (21 175)	268 (61 908)	220 (16 940)	7 (539)
Ammonium and Methylamine					
275	20	53 (1060)	66 (3760)	41 (820)	5 (100)
250	20	66 (1320)	67 (4020)	670 (13 400)	8 (160)
225	20	114 (2280)	67 (4060)	—[d]	12 (240)
200	20	111 (2220)	121 (6440)	738 (14 760)	18 (360)
100	20	76 (1520)	88 (5160)	—[d]	100 (2000)
200	77	248 (19 096)	—[d]	—[d]	16 (1232)
H + Benzene					
275	20	127 (2540)	119 (6080)	263 (5260)	5 (100)
250	20	129 (2580)	123 (6160)	82 (1640)	6 (120)
225	20	142 (2840)	124 (6540)	133 (2660)	10 (200)
200	20	225 (4500)	104 (5480)	258 (5160)	17 (340)
100	20	—[b]	75 (4080)	652 (13 040)	44 (880)
200	77	528 (40 656)	463 (106 953)	—[d]	19 (1463)

[a] While $g_{tol} = 10^{-7}$ and number of energy and gradient evaluations in parentheses. All calculations started out from a converged instanton at T = 300 K, P = 20. [b] Calculation converged to a wrong stationary point (all images in the reactant minimum). [c] Calculation converged to a wrong stationary point (images interchanged during the optimization). [d] Not converged.

being zero. Using $\Delta r = 0.6$, as defined in eq 10, leads to convergence to a delocalized Feynman path, the instanton.

Further instantons at lower temperature were optimized starting from the geometry and the Hessian of the instanton obtained with TM at 300 K. Here we tested the convergence for different temperature intervals rather than using sequential cooling. For T = 200 K we additionally performed an instanton search with more images, P = 77. We interpolated geometries and Hessians from the instanton with P = 20 and T = 300 K by inserting three extra images in between two consecutive ones.

The number of steps needed to achieve convergence in each case, along with the number of energy and gradient evaluations needed, are given in Table 2. The convergence behavior is exemplary depicted in Figure 3.

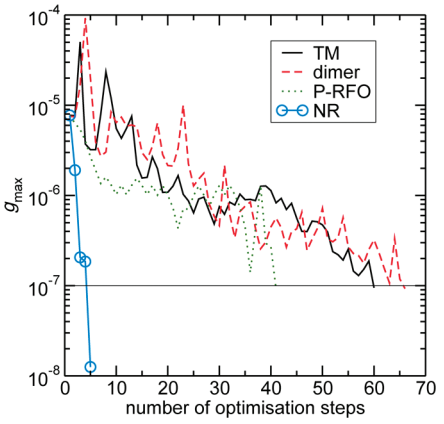

Figure 3. Convergence behavior of the four different optimization methods for ammonium and methylamine at T = 275 K. NR converges almost quadratically. The convergence criterion of $g_{max} = g_{tol} = 10^{-7}$ is indicated by a thin horizontal line.

In TM, P-RFO, and NR the number of energy evaluations is P times the number of optimization steps. In the dimer method, the rotations require additional energy evaluations. At least two energy and gradient calculations of the full path (dimer mid- and end-points) are required for an estimate of the rotational angle.[77] In most iterations, at least a third calculation (one dimer rotation) was required. Especially at the beginning of an optimization run, more dimer rotations may be necessary. Overall, in the dimer optimizations, the number of energy and gradient evaluations is about $3P$ times the number of optimization steps. This indicates that on average one dimer rotation step per iteration was sufficient.

Those cases for which numbers are given in Table 2 converged to the correct instanton within a maximum of 1000 optimization steps and 200 000 energy evaluations. Consistency was checked by comparing S_E, S_0, and k_{inst} as well as the eigenvalue spectrum between the results of different optimization algorithms.

For the H + benzene case, the initial instanton search for T = 300 K with the TM method resulted in a somewhat problematic starting structure for the following instanton optimizations. The reason being that for this system the potential energy surface is very flat close to the reactant minimum. This results in many of the images accumulating there. A too weak convergence criterion leads to numerical noise in the image positions and, thus, to numerical noise in $\mathbf{u}_{inst}$ in the TM method. Thus, for the TM calculations of this system, the instanton at T = 300 K optimized with NR was used as the starting geometry.

The influence of P and g_{tol} on the vibrational instanton rates $[\log_{10}(k_{inst})]$, ignoring changes in the rotational partition function as well as the translational partition function between the reactant and the instanton, is shown in Table 3. The error relative to the most accurate value obtained with P = 96 images and $g_{tol} = 10^{-9}$ is given. A difference in the logarithm of 0.1 corresponds to a rate which is off by about 25.9%.

The ammonium and methylamine case raises a particular issue in the rate calculations. The "vibrational" mode in which the two fragments rotate with respect to each other has a very low vibrational frequency of only 11.5 cm^{-1} at the classical TS. Thus, at the temperature range considered, this mode would better be described as a hindered rotator than as a harmonic oscillator. Since in this work we only investigate the effect of

Table 3. Error in the Logarithm of the Rates Compared to the Tightest Convergence Criterion g_{tol} and the Largest Number of Images for Each Case (T = 200 K, NR)

	g_{tol}				
P	10^{-5}	10^{-6}	10^{-7}	10^{-8}	10^{-9}
Malonaldehyde					
20	−0.05	−0.01	−0.01	0.00	0.00
39	−0.14	−0.15	0.00	0.00	0.00
58	−0.53	−0.00	0.00	0.00	0.00
77	−0.54	−0.10	−0.01	0.00	0.00
96	−0.19	−0.10	−0.01	0.00	0.00
Ammonium and Methylamine					
20	−0.45	−0.01	−0.01	−0.01	−0.01
39	−0.20	−0.01	0.00	0.00	0.00
58	−0.18	−0.27	0.00	0.00	0.00
77	−0.19	−0.41	0.00	0.00	0.00
96	−0.20	−0.40	0.00	0.00	0.00
H + Benzene					
20	0.14	0.25	0.01	0.01	0.01
39	0.18	0.31	0.00	0.00	0.00
58	0.17	−0.05	−0.01	0.00	0.00
77	0.10	0.31	0.00	0.00	0.00
96	0.21	0.29	0.01	0.00	0.00

P and g_{tol} on the rates, in Table 3 we ignored this mode just as the other six translational and rotational modes are ignored. If it were included as a vibrational mode in the rate calculations, then its low eigenvalue would cause numerical problems in automatically designating the real zero eigenvalues in the eigenvalue spectrum of the instanton Hessian, thereby compromising the rates. It is worth noting at this point that the additional low mode was handled well by the optimization algorithms.

V. DISCUSSION

We compared four different algorithms to optimize instantons. The results clearly show that the NR algorithm is the most promising one among those tested. Its near-quadratic convergence results in only few optimization steps necessary to reach tight convergence criteria. The convergence behavior is also promising for applications to systems with significantly more degrees of freedom. The methods are not restricted to sequential cooling. Using analytic potentials, we achieved convergence even with the TM method for a straight-line path as starting guess (data not shown). In these cases, a Hessian from previous calculations is not easily available. The results also point out some problems which can be expected in instanton optimizations. These will now be addressed.

It is clear from Table 2 that the P-RFO fails to converge in a number of cases. As a fixed-point iteration scheme, it sometimes reaches a periodic cycle rather than actually converging to the desired stationary point. This can be seen by plotting the maximum gradient component against the number of iterations, see Figure 4. In all cases except T = 100 K, a cycle is reached rather than the gradient becoming smaller and smaller. This is caused by a strong dependence of the P-RFO algorithm on an accurate Hessian. In our approach, we only update the Hessian of

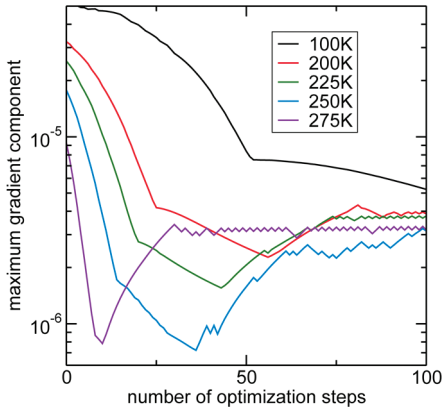

Figure 4. Convergence failures of the P-RFO method for malonaldehyde at different temperatures.

the individual images rather than recalculating it, which inevitably leads to inaccuracies. Using the Powell update[98] or no update scheme at all leads to an even worse convergence (data not shown). Recalculating the Hessian in each step would of course be prohibitively expensive. Since the other algorithms, in particular NR, generally converge faster and more reliably, instanton optimization with P-RFO is not recommended.

NR intrinsically converges to any stationary point, not necessarily first-order saddle points. While in all results shown here, it actually converged to the sought-after instanton; we observed runs in which NR converged to different states. Especially at high temperature, close to T_c, there seems to be a danger of the whole path collapsing to the classical TS. This was observed here when starting from the classical TS and searching for an instanton at T = 300 K in the case of malonaldehyde. A larger Δr for spreading the images in the initial path resolved that problem.

Convergence to a collapsed path can easily be detected during an optimization run by a steadily decreasing value of S_0. According to eq 8, S_0 vanishes for any collapsed path. In cases where NR converges to a different stationary point than the instanton, the TM algorithm is recommended as a backup solution.

In two cases, H + benzene at T = 100 K with the TM method and the dimer method, the calculations actually converged to a path collapsed to the reactant state, see Table 2. While this is also a stationary point of S_E, it obviously is no instanton. These cases are less worrying, however, because the direct change from T = 300 K (starting point) to T = 100 K is rather extreme. Smaller temperature intervals are recommended. Even at this large temperature interval, however, NR converged well.

Convergence criteria are applied in our present implementation in the same unit system as the optimization being done, i.e., in mass-weighted coordinates with the mass of an electron as unit. To assess which g_{tol} is necessary to obtain the tunneling rate with a given accuracy, we calculated the data presented in Table 3. A criterion of $g_{tol} = 10^{-7}$ seems sufficient to ensure convergence of the logarithm (basis 10) of the rate to within 0.01. For the systems and the temperature (T = 200 K) studied here, P = 20 images are obviously sufficient, as the rate (at sufficiently small g_{tol}) is independent of the number of images. At lower temperature, however, the images become less equally spaced in configuration space. More and more images accumulate close to the minima. In these cases, more images are required to achieve converged rates as found in agreement with previous work.[49] It can also be seen from Table 3 that with more and more images,

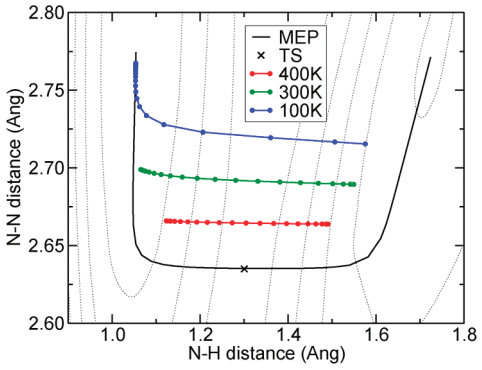

Figure 5. The potential energy surface, the MEP, and instantons at three temperatures for the case of ammonium and methylamine, projected onto a plane of two geometric coordinates. The corner cutting shortens the tunneling path by keeping the heavy nitrogen atoms fixed and focusing the movement onto the light hydrogen atom.

the rate becomes more sensitive to g_{tol}. At 20 images, the rate is already converged if $g_{tol} = 10^{-6}$ is used for malonaldehyde and ammonium and methylamine.

The remaining error at nonperfect convergence can be due to three sources, $k_{inst} = k_{S_0} \cdot k_{harm} \cdot k_{S_E}$, as apparent from eq 7 with S_0 (entering the rate as $k_{S_0} = (S_0/(2\pi\hbar))^{1/2}$, S_E (entering the rate as $k_{S_E} = \exp(-S_E/\hbar)$, and all terms covering the quadratic expansion of the potential around the stationary paths: $k_{harm} = (1/Q_{RS})(P'/\beta\hbar)(1/(|\Pi_i' \lambda_i|)^{1/2})$. The latter causes the largest effect. This is somewhat surprising as S_E enters the rate exponentially. The eigenvalues λ_i of the Hessian only enter under the square root. However, numerical noise in the Hessian affects most or all eigenvalues, which together apparently make a noticeable contribution. Thus, it seems important to calculate the Hessians of the images with high accuracy.

Finally, we discuss a property of the instanton path itself rather than the optimization of it, namely corner cutting. Tunneling is more efficient the thinner the barrier is. The relevant width of the barrier is the width in mass-weighted (or any iso-inertial) coordinates. Thus, movement of heavy atoms reduces the tunneling rate more than movement of light atoms. This results in an instanton path which, in many cases, deviates significantly from the MEP, an effect known as corner cutting.[27] An example is demonstrated in Figure 5. The figure shows the N−N distance plotted against one N−H distance of the ammonium and methylamine system used in this work. All numbers are of course calculated with semiempirical methods of limited accuracy. However, the qualitative conclusions also hold with more accurate methods. On the MEP, the nitrogen atoms approach each other significantly (shortening of the N−N distance by 0.14 Å) before the hydrogen atom is transferred. The movement of the heavy atoms is more and more avoided the more important tunneling becomes. At $T = 100$ K, the N−N distance decreases by only 0.06 Å. This shortening of the effective tunneling path comes at the expense of a higher energy of some images along the instanton compared to the classical TS. However, it still results in a larger tunneling rate than tunneling along the MEP.

VI. CONCLUSION

We presented a comparison of four newly implemented methods to search for instantons as saddle points on the Euclidean action surface spanned by closed Feynman paths. NR turned out to be consistently efficient and stable. The methods were tested at various temperatures for three different small chemical systems with tunneling hydrogen atoms. We applied semiempirical methods to obtain the quantum chemical potential energies and forces. However, preliminary tests showed that the same conclusions are reached for density functional theory (DFT) calculations.

We will continue to apply these algorithms to chemically relevant systems using more accurate quantum chemical methods. Preliminary results show that the methods are also applicable to enzymatic systems with many degrees of freedom described by a QM/MM energy expression.[59]

The results of this work show that instantons can be optimized rather efficiently. The geometry optimization generally requires less energy and gradient evaluations than subsequent Hessian calculations at each image, at least if the latter are done by finite-difference calculations of gradients using the two-point formula. Efficiency in the Hessian calculations can of course be gained by using analytic Hessians instead. Additionally, it may be of interest to find methods to calculate the rate using the Hessian at fewer points along the instanton. Accuracy can be improved by calculating the energies of the points along the instanton path with a higher level of theory, while performing the optimization and the Hessian calculations at the lower level. An additional challenge in instanton theory is the issue that at lower temperature, more and more images of the discretized path tend to accumulate at one end of the instanton path (the one with the smaller slope of the energy along the path). Up to some point, this can be accounted for by using more and more images. However, to apply instanton theory to really low temperature, or to calculate the limit at $T \rightarrow 0$, different schemes will have to be developed.

AUTHOR INFORMATION

Corresponding Author

*E-mail: kaestner@theochem.uni-stuttgart.de.

ACKNOWLEDGMENT

J.B.R. and J.K. thank the German Research Foundation (DFG) for financial support of the project within the Cluster of Excellence in Simulation Technology (EXC 310/1) at the University of Stuttgart. T.P.M.G. thanks The Netherlands Organization for Scientific Research (NWO) for a VENI-fellowship (700.58.404). The work was stimulated by an HPC-Europa2 project awarded to T.P.M.G. to visit J.K. Prof. H. Jónsson and Dr. A. Arnaldsson are acknowledged for helpful discussions.

REFERENCES

(1) Gamow, G. *Z. Phys.* **1928**, 204.
(2) Eckart, C. *Phys. Rev.* **1930**, *35*, 1303.
(3) Cazaux, S.; Caselli, P.; Cobut, V.; Le Bourlot, J. *Astron. Astrophys.* **2008**, *483*, 495–508.
(4) Goumans, T. P. M.; Kästner, J. *Angew. Chem., Int. Ed.* **2010**, *49*, 7350–7352.
(5) Goumans, T. P. M.; Kästner, J. *Angew. Chem.* **2010**, *122*, 7508–7511.
(6) Liang, Z.-X.; Klinman, J. P. *Curr. Opin. Struct. Biol.* **2004**, *14*, 648.
(7) Bandaria, J. N.; Cheatum, C.; Kohen, A. *J. Am. Chem. Soc.* **2009**, *131*, 10151–10155.
(8) Masgrau, L.; Roujeinikova, A.; Johannissen, L. O.; Hothi, P.; Basran, J.; Ranaghan, K. E.; Mulholland, A. J.; Sutcliffe, M. J.; Scrutton, N. S.; Leys, D. *Science* **2006**, *312*, 237–241.

(9) Yoon, M.; Song, H.; Håkansson, K.; Marsh, E. N. G. *Biochemistry* **2010**, *49*, 3168–3173.
(10) Grant, K. L.; Klinman, J. P. *Biochemistry* **1989**, *28*, 6597.
(11) Knapp, M. J.; Klinman, J. P. *Eur. J. Biochem.* **2002**, *269*, 3113–3121.
(12) Antoniou, D.; Caratzoulas, S.; Kalyanaraman, C.; Mincer, J. S.; Schwartz, S. D. *Eur. J. Biochem.* **2002**, *269*, 3103–3112.
(13) Klinman, J. P. *J. Biol. Chem.* **2006**, *281*, 3013.
(14) Sutcliffe, M. J.; Scrutton, N. S. *Eur. J. Biochem.* **2002**, *269*, 3096.
(15) Masgrau, L.; Roujeinikova, A.; Johannissen, L. O.; Hothi, P.; Basran, J.; Ranaghan, K. E.; Mulholland, A. J.; Sutcliffe, M. J.; Scrutton, N. S.; Leys, D. *Science* **2006**, *312*, 237.
(16) Wang, M.; Lu, Z.; Yang, W. *J. Chem. Phys.* **2006**, *124*, 124516.
(17) Bothma, J. P.; Gilmore, J. B.; McKenzie, R. H. *New J. Phys.* **2010**, *12*, 055002.
(18) Arrhenius, S. *Z. Phys. Chem. (Leipzig)* **1889**, *4*, 226.
(19) Eyring, H.; Polanyi, M. *Z. Phys. Chem., Abt. B* **1931**, 279.
(20) Hänggi, P.; Talkner, P.; Borkovec, M. *Rev. Mod. Phys.* **1990**, *62*, 251.
(21) Pollak, E.; Talkner, P. *Chaos* **2005**, *15*, 026116.
(22) Wigner, E. P. *Z. Phys. Chem.* **1932**, *15*, 203.
(23) Bell, R. The application of tunnel corrections in chemical kinetics. In *The tunnel effect in chemistry*; 1st ed.; Chapman and Hall: London, 1980; Vol. 1, pp 51−140.
(24) Gillan, M. *J. Phys. C: Solid State Phys.* **1987**, *20*, 3621.
(25) Wigner, E. *Trans. Faraday Soc.* **1938**, *34*, 29.
(26) Kuppermann, A.; Truhlar, D. *J. Am. Chem. Soc.* **1971**, *93*, 1840–1851.
(27) Marcus, R. A.; Coltrin, M. E. *J. Chem. Phys.* **1977**, *67*, 2609.
(28) Skodje, R.; Truhlar, D.; Garrett, B. *J. Phys. Chem.* **1981**, *85*, 3019–3023.
(29) Garrett, B. C.; Truhlar, D. G.; Wagner, A. F.; Thom H. Dunning, J. *J. Chem. Phys.* **1983**, *78*, 4400–4413.
(30) Garrett, B. C.; Abusalbi, N.; Kouri, D. J.; Truhlar, D. G. *J. Chem. Phys.* **1985**, *83*, 2252–2258.
(31) Liu, Y. P.; Lu, D. H.; Gonzalez-Lafont, A.; Truhlar, D. G.; Garrett, B. C. *J. Am. Chem. Soc.* **1993**, *115*, 7806–7817.
(32) Meana-Pañeda, R.; Truhlar, D. G.; Fernández-Ramos, A. *J. Chem. Theory Comput.* **2010**, *6*, 6–17.
(33) Langer, J. S. *Ann. Phys. (N.Y.)* **1967**, *41*, 108.
(34) Miller, W. H. *J. Chem. Phys.* **1975**, *62*, 1899.
(35) Coleman, S. *Phys. Rev. D: Part. Fields* **1977**, *15*, 2929.
(36) Callan, C. G., Jr.; Coleman, S. *Phys. Rev. D: Part. Fields* **1977**, *16*, 1762.
(37) Gildener, E.; Patrascioiu, A. *Phys. Rev. D: Part. Fields* **1977**, 423.
(38) Feynman, R. P. *Rev. Mod. Phys.* **1948**, *20*, 367.
(39) Mills, G.; G. K. Schenter, D. M.; Jónsson, H. RAW Quantum Transition State Theory. In *Classical and Quantum Dynamics in Condensed Phase Simulations*; 1st ed.; Berne, B. J., Ciccotti, G., Coker, D. F., Eds.; World Scientific Press: Hackensack, NJ, 1998; Vol. 1, pp 405−421.
(40) Miller, W. H.; Zhao, Y.; Ceotto, M.; Yang, S. *J. Chem. Phys.* **2003**, *119*, 1329.
(41) Vaníček, J.; Miller, W. H.; Castillo, J. F.; Aoiz, F. J. *J. Chem. Phys.* **2005**, *123*, 054108.
(42) Chapman, S.; Garrett, B. C.; Miller, W. H. *J. Chem. Phys.* **1975**, *63*, 2710.
(43) Mills, G.; Jónsson, H. *Phys. Rev. Lett.* **1994**, *72*, 1124.
(44) Mills, G.; Jónsson, H.; Schenter, G. K. *Surf. Sci.* **1995**, *324*, 305–337.
(45) Mills, G.; Schenter, G. K.; Makarov, D. E.; Jónsson, H. *Chem. Phys. Lett.* **1997**, *278*, 91.
(46) Siebrand, W.; Smedarchina, Z.; Zgierski, M. Z.; Fernández-Ramos, A. *Int. Rev. Phys. Chem.* **1999**, *18*, 5.
(47) Smedarchina, Z.; Siebrand, W.; Fernández-Ramos, A.; Cui, Q. *J. Am. Chem. Soc.* **2003**, *125*, 243–251.
(48) Qian, T.; Ren, W.; Shi, J.; E, W.; Shen, P. *Physica A* **2007**, *379*, 491.
(49) Andersson, S.; Nyman, G.; Arnaldsson, A.; Manthe, U.; Jónsson, H. *J. Phys. Chem. A* **2009**, *113*, 4468.
(50) Goumans, T. P. M.; Andersson, S. *Mon. Not. R. Astron. Soc.* **2010**, *406*, 2213–2217.
(51) Manthe, U.; Meyer, H.-D.; Cederbaum, L. S. *J. Chem. Phys.* **1992**, *97*, 3199–3213.
(52) Meyer, H.-D.; Manthe, U.; Cederbaum, L. *Chem. Phys. Lett.* **1990**, *165*, 73–78.
(53) Padmanaban, R.; Nest, M. *Chem. Phys. Lett.* **2008**, *463*, 263–266.
(54) Hammer, T.; Coutinho-Neto, M. D.; Viel, A.; Manthe, U. *J. Chem. Phys.* **2009**, *131*, 224109.
(55) Hansen, N. F.; Andersen, H. C. *J. Phys. Chem.* **1996**, 1137.
(56) Cheney, B. G.; Andersen, H. C. *J. Chem. Phys.* **2003**, *118*, 9542–9551.
(57) Cao, J.; Voth, G. A. *J. Chem. Phys.* **1994**, 6157.
(58) Voth, G. A. *Adv. Chem. Phys.* **1996**, 135.
(59) Pollak, E.; Liao, J.-L. *J. Chem. Phys.* **1998**, 2733.
(60) Richardson, J. O.; Althorpe, S. C. *J. Chem. Phys.* **2009**, *131*, 214106.
(61) Craig, I. R.; Manolopoulos, D. E. *J. Chem. Phys.* **2005**, *122*, 084106.
(62) Voth, G. A.; Chandler, D.; Miller, W. H. *J. Chem. Phys.* **1989**, 7749.
(63) Voth, G. A. *J. Phys. Chem.* **1993**, 8365.
(64) Simon, B. *Functional integration and quantum physics*; 2nd ed.; Academic Press: New York, 1979; Vol. 1;
(65) Arnaldsson, A. Ph.D. thesis, University of Washington: Seattle, WA, 2007.
(66) Mestela, B.; Percival, I. *Physica D* **1987**, *24*, 172.
(67) Baranger, M.; Davies, K. T. R.; Mahoney, J. H. *Ann. Phys. (N.Y.)* **1988**, *186*, 95.
(68) Grobgeld, D.; Pollak, E.; Zakrzewski, J. *Physica D* **1992**, *56*, 368.
(69) Marcinek, R.; Pollak, E. *J. Chem. Phys.* **1994**, *100*, 5894.
(70) Messina, M.; Schenter, G. K.; Garrett, B. C. *J. Chem. Phys.* **1995**, *103*, 3430.
(71) Kästner, J.; Carr, J. M.; Keal, T. W.; Thiel, W.; Wander, A.; Sherwood, P. *J. Phys. Chem. A* **2009**, *113*, 11856.
(72) Kästner, J.; Keal, T. W.; Sherwood, P. *DL-FIND*; CCPForge: Daresbury Lab, United Kingdom; http://ccpforge.cse.rl.ac.uk/gf/project/dl-find/. Accessed November 15, 2010.
(73) Sherwood, P.; de Vries, A. H.; Guest, M. F.; Schreckenbach, G.; Catlow, C. R. A.; French, S. A.; Sokol, A. A.; Bromley, S. T.; Thiel, W.; Turner, A. J.; Billeter, S.; Terstegen, F.; Thiel, S.; Kendrick, J.; Rogers, S. C.; Casci, J.; Watson, M.; King, F.; Karlsen, E.; Sjøvoll, M.; Fahmi, A.; Schäfer, A.; Lennartz, C. *J. Mol. Struct. (THEOCHEM)* **2003**, *632*, 1.
(74) *ChemShell, a Computational Chemistry Shell*; Computational Science and Engineering Department: Daresbury Lab, United Kingdom; http://www.chemshell.org. (Accessed November 15, 2010)
(75) Henkelman, G.; Jónsson, H. *J. Chem. Phys.* **1999**, *111*, 7010.
(76) Olsen, R. A.; Kroes, G. J.; Henkelman, G.; Arnaldsson, A.; Jónsson, H. *J. Chem. Phys.* **2004**, *121*, 9776.
(77) Heyden, A.; Bell, A. T.; Keil, F. J. *J. Chem. Phys.* **2005**, *123*, 224101.
(78) Kästner, J.; Sherwood, P. *J. Chem. Phys.* **2008**, *128*, 014106.
(79) Liu, D. C.; Nocedal, J. *Math. Program* **1989**, *45*, 503.
(80) Nocedal, J. *Math. Comp.* **1980**, *35*, 773.
(81) Broyden, C. G. *IMA J. Appl. Math.* **1970**, *6*, 76.
(82) Fletcher, R. *Comp. J.* **1970**, *13*, 317.
(83) Goldfarb, D. *Math. Comp.* **1970**, *24*, 23.
(84) Shanno, D. F. *Math. Comp.* **1970**, *24*, 647.
(85) Lanczos, C. *J. Res. Nat. Bur. Stand* **1951**, *45*, 255–282.
(86) Malek, R.; Mousseau, N. *Phys. Rev. E: Stat. Phys., Plasmas, Fluids, Relat. Interdiscip. Top.* **2000**, *62*, 7723.
(87) Cerjan, C. J.; Miller, W. H. *J. Chem. Phys.* **1981**, *75*, 2800.
(88) Simons, J.; Jørgensen, P.; Taylor, H.; Ozment, J. *J. Phys. Chem.* **1983**, *87*, 2745.

(89) Banerjee, A.; Adams, N.; Simons, J.; Shepard, R. *J. Phys. Chem.* **1985**, *89*, 52–57.
(90) Baker, J. *J. Comput. Chem.* **1986**, *7*, 385–395.
(91) Bofill, J. M. *J. Comput. Chem.* **1994**, *15*, 1.
(92) Stewart, J. J. P. *J. Comput. Chem.* **1989**, *10*, 209.
(93) Wong, K. F.; Sonnenberg, J. L.; Paesani, F.; Yamamoto, T.; Vaníček, J.; Zhang, W.; Schlegel, H. B.; Case, D. A.; Cheatham, T. E., III; Miller, W. H.; Voth, G. A. *J. Chem. Theory Comput* **2010**, *6*, 2566.
(94) Dewar, M. J. S.; Zoebisch, E. G.; Healy, E. F.; Stewart, J. J. P. *J. Am. Chem. Soc.* **1985**, *107*, 3902.
(95) Grimme, S. *J. Comput. Chem.* **2006**, *27*, 1787.
(96) Thiel, W. *MNDO99*, v. 6.1; Max-Planck-Institut für Kohlenforschung: Mülheim an der Ruhr, Germany, 2004.
(97) Humphrey, W.; Dalke, A.; Schulten, K. *J. Molec. Graphics* **1996**, *14*, 33.
(98) Powell, M. J. D. *Math. Prog.* **1971**, *26*, 1.
(99) Rommel, J. B.; Kästner, J. to be published.